A Hybrid Statistical IHS Image Fusion Method

Ali Reza Afary[1], Mohammad Javad Valdan Zoej[2], Hassan Emami[3]
[1]Ali Reza Afary, Babol University of Technology, Babol, Iran (E-mail: afary@nit.ac.ir)
[2]Mohammad Javad Valdan Zoj, K.N. Toosi University of Technology, Tehran, Iran
(E-mail: valadanzouj@kntu.ac.ir)
[3]Hassan Emami, University of Tabriz, Tabriz, Iran (E-mail: h_emami@tabrizu.ac.ir)

Abstract:
IHS method for image fusion is one of the conventional methods with a simple theory. Implementation of this method is simple and effective from computational point of view. But this method causes the spectral content of the fused image to get disturbed in comparison with the spectral criteria of the main multispectral image. In this article a statistical image fusion method is combined with the conventional IHS method to improve its spectral quality and overcome its deficiency. Some spectral indices were used for evaluation of this combined method and compared with the conventional IHS and the used statistical fusion methods. This combined method improves the spectral quality of the fused image and eliminates the existing shortcomings of the spectral disturbing in fused image produced by IHS method.

Keywords: *Image fusion, IHS, Statistical method, Spectral quality.*

1. Introduction

Remote sensing satellites take images at different spatial, spectral and temporal resolutions from earth surface in different parts of the electromagnetic spectrum. The aim of satellite image fusion is to unite their spatial, spectral and temporal information, and also to increase their reliability in order to increase interpretability. In the act of fusing multispectral satellite images (*XS*), having high spectral and low spatial resolutions, with a panchromatic image (*PAN*), having high spatial resolution, the final production must be the same as the image took simultaneously by a sensor with the same spectral resolution of *XS* image and spatial resolution of *PAN* image [1,2]. Image geo-referencing or image to image registration, and resampling of *XS* image into the spatial pixel dimensions of *PAN* image, is one of the primary and main parts of the image fusion process [3]. If the images used in the fusion process have not been taken simultaneously, it will be necessary to apply a series of radiometric corrections such as the histogram matching of *PAN* image histogram with the histogram of the Intensity element of *XS* image. Image fusion may be done in three levels of pixel, object and decision making [3]. This article is on the pixel level image fusion.

1.1 The Studied Region and Data

Three data sets were used in this article; *QuickBird* (*PAN* and *XS*), *Worldview-02* (*PAN* and *XS*), and *EO1-ALI* (*PAN* band) with *Landsat TM*(Fig.s 1-6). Because of the limitation of custom *IHS* method in accepting only three bands of *XS* image [3], just three bands from multispectral images were selected and used in fusion process. TABLE I is showing the criteria of all data sets that are used in this article. Dimensions of the studied *PAN* and *XS* images (after resampling *XS* image to corresponding *PAN* image pixel size) are 1024×1024 pixels.

1.2 IHS Image Fusion Method

This method is a spectral substituting method in pixel level which is done by transforming of XS image from the RGB color space to IHS color space and substituting its spatial element, Intensity, with PAN image and then doing the reverse IHS transform and coming back to the RGB color space [3-6].

1.3 IHS Color Space

In image processing, *IHS* colored space is used as a means for separating spatial element, *Intensity*, from spectral elements, *Hue* and *Saturation*, of a three banded image. There are different methods to accomplish this separation [3-10]. In this research transforming from *RGB* color space to *IHS* and vice versa is done through Equations (1) and (2) [9]. From among different methods of computing *Intensity* element in *IHS* transformation, using Equation (1) will end in better results [10], which is also used in this research. The fused images using *IHS* method have been shown in Fig.s 7-9.

$$\begin{bmatrix} I \\ v_1 \\ v_2 \end{bmatrix} = \begin{bmatrix} \frac{1}{3} & \frac{1}{3} & \frac{1}{3} \\ \frac{-1}{\sqrt{6}} & \frac{-1}{\sqrt{6}} & \frac{2}{\sqrt{6}} \\ \frac{1}{\sqrt{6}} & \frac{-1}{\sqrt{6}} & 0 \end{bmatrix} \begin{bmatrix} R \\ G \\ B \end{bmatrix}; \quad \begin{cases} H = \tan^{-1}\left(\frac{v_2}{v_1}\right) \\ S = \sqrt{v_1^2 + v_2^2} \end{cases} \tag{1}$$

$$\left.\begin{matrix} v_1 = S\cos(H) \\ v_2 = S\sin(H) \end{matrix}\right\} \Rightarrow \begin{bmatrix} R \\ G \\ B \end{bmatrix} = \begin{bmatrix} 1 & \frac{-\sqrt{6}}{6} & \frac{\sqrt{6}}{2} \\ 1 & \frac{\sqrt{6}}{6} & \frac{-\sqrt{6}}{2} \\ 1 & \frac{\sqrt{6}}{3} & 0 \end{bmatrix} \begin{bmatrix} I \\ v_1 \\ v_2 \end{bmatrix} \tag{2}$$

table i: Criteria of Data Sets Used in this Article

Sensor	**QuikBird (PAN & XS)**				**Worldview-02 (PAN & XS)**				**EO1-ALI (PAN) and Landsat TM5 (XS)**			
	PAN	R = B4	G = B3	B = B2	PAN	R = B7	G = B5	B = B3	PAN (ALI)	R = B4	G = B3	B = B2
Wavelength (µm)	0.50–0.90	0.76-0.90	0.63-0.69	0.52-0.60	0.45-0.80	0.770-0.895	0.630-0.690	0.51-0.58	0.48-0.69	0.76-0.90	0.63-0.69	0.52-0.60
Pixel Size (m)	0.6	2.4			0.5	2			10	30		
Date of Acquisition	2009-05-22				2010-06-14				2010-05-30	2010-09-11		
Bits Per Pixel	8				8				8			
Coordinate System	UTM Z39N (WGS84)				UTM Z39N (WGS84)				UTM Z38N (WGS84)			
Location	Marvdasht near Shiraz city of Iran				Tehran City, Capital of Iran				Urmia City of Iran			

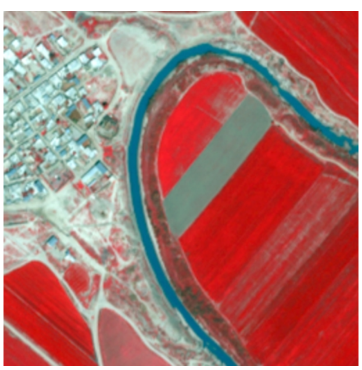

Fig 1: QuikBird XS image (B432)

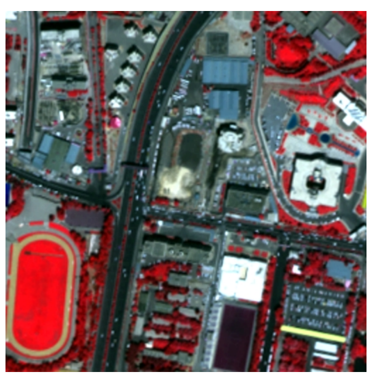

Fig 2: WorldView-02 XS image (B753)

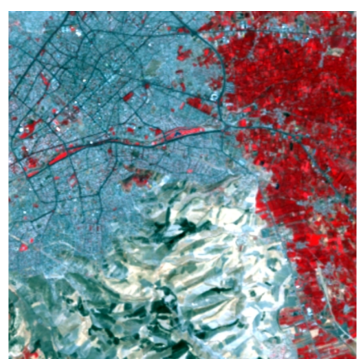

Fig 3: Landsat TM5 XS image (B432)

Fig 4: QuickBird PAN image

Fig 5: WorldView-2 PAN image

Fig 6: EO1-ALI PAN image

2. A Review on IHS Fusion Method

In the first *IHS* based image fusion procedure, proposed by *Haydn et al* in 1982 [11], the *Intensity* component of *XS* image was directly replaced with the *PAN* image. It is known that although this method provides fused images with enhanced spatial quality, their spectral information differs significantly from that of the original multispectral ones. Image fusion with *IHS* method has some disadvantages and commonly distorts the spectral quality of the fused image in comparison with the main multispectral image, especially in *Green* and *Near Infra-Red* (*NIR*) bands [4,5,12]. Besides, this fusion method when applied on images with different resolutions, lead to different results [13]. Different approaches have been proposed during the last decades to minimize the spectral distortion inherent to IHS fusion method. To decrease the spectral distortion, some methods such as histogram matching of *PAN* image with *Intensity* element of *XS* image are used [14]. Also stretching of *Hue* and *Saturation* elements before reverse transformation is suggested [14]. On the other hand the quality of the fused image in *IHS* method relates also to the sensor bandwidth of *PAN* image. In these methods, the best result is obtained when sensor band width of *PAN* image covers the whole sensor bandwidth of *XS* image like *PAN* sensor of *Ikonos, QuickBird* and *WorldView-2* images [4, 15,16]. To overcome these problems some authors [10,17] proposed to combine *IHS* method with multiresolution wavelet fusion method and inject, into the *Intensity* image, the spatial information of the *PAN* image, missing into the multispectral one, in a multiresolution wavelet frame. The wavelet coefficients of the *PAN* image, which pick up the spatial information of this one, are extracted using wavelet algorithm. This method is capable of enhancing the spatial quality of the multispectral image while preserving its spectral information. The wavelet method does not modify the total radiance of the *XS* image since the mean value of each of the wavelet coefficients is zero [10]. Taking into account the computational cost of the wavelet fusion method, as well as the methods proposed by *Chibani* and *Houacine* [18], *Choi* [19] proposed proposed an alternative *IHS* based simplified procedure. In this case, the new *Intensity* image is obtained as a combination of the *Intensity* and *PAN* images and the tradeoff between the spatial and spectral resolution of the images to be fused can be controlled using a tradeoff parameter (t) [19].

Another shortcoming of *IHS* method is its limitation in using just three bands of *XS* image in the fusion process, accordingly the suitable bands must be chosen from among different bands of *XS* image [20]. For example, in *Landsat ETM+* (7 bands), *WorldView-02* (8 bands) and *QuickBird* (4 bands) images, just three bands of *XS* image must be selected for fusing with *IHS* method. In order to extend the *IHS* based image fusion methods, from three to n-bands, *Tu et al.* [4,5] proposed a new Generalized *IHS* fusion method.

3. Statistical Image Fusion Method

The Statistical image fusion Method - represented by *ST* symbol as follows - which is combined in this research with the *IHS* method to improve its spectral quality is based on the method presented by *Gungor* and *Shan* [21]. This approach constructs the fused images as a linear combination of the *PAN* and *XS* images through Equation (3) in which *i* and *j* are the row and column numbers of each pixel and *k* is the band number of the *XS* and fused image *F*, and *N* is the total number of the bands in the *XS* image.

$$F_{ij}^{k} = a_{ij}^{k} \times PAN_{ij} + b_{ij}^{k} \times XS_{ij}^{k} \quad ; \quad k = 1, 2, ..., N \tag{3}$$

Any pixel in the *k*th band of fused image is obtained by multiplying the corresponding pixels of *PAN* and *XS* images respectively by *a* and *b*, the weighting coefficients, and calculating the sum of the products. For any pixel, the coefficients *a* and *b* must be determined window by window *i.e.* for calculating these coefficients in Equation (3), first two windows having $w \times w$ dimensions is defined around any corresponding pixel in *PAN* image and in the *k*th band of *XS* image [21].

Padding process will be needed for the border regions of the input images. There are various padding approaches in the literature and in this study the zero padding approach which extends the images with zeros was used. On the basis of Digital Number (*DN*) values of pixels included in these windows and the statistical relations obtained from the two below criteria, the coefficients *a* and *b* are calculated [21]:

The first criteria: The mean of every fused image band should be equal the average of its corresponding *XS* image band.

$$m_{F_{ij}^{k}} = a_{ij}^{k} \times m_{PAN_{ij}} + b_{ij}^{k} \times m_{XS_{ij}^{k}} = m_{XS_{ij}^{k}} \tag{4}$$

Where $m_{F_{ij}^{k}}$ is the mean of fused image in the *k*th band, is the mean of *PAN* image, and $m_{PAN_{ij}}$ is the mean of *XS* image in the *k*th band.

The second criteria: The variance of every band in a fused image should be equal with the variance of *PAN* image.

$$s_{F_{ij}^{k}}^{2} = \left(a_{ij}^{k}\right)^{2} s_{PAN_{ij}}^{2} + 2 \times a_{ij}^{k} \times b_{ij}^{k} \times s_{PAN_{ij}, XS_{ij}^{k}} + \left(b_{ij}^{k}\right)^{2} s_{XS_{ij}^{k}}^{2} = s_{PAN_{ij}}^{2} \tag{5}$$

Where $s_{F_{ij}^{k}}^{2}$, is the variance of fused image *F* in the *k*th band, $s_{PAN_{ij}}^{2}$, is the variance of *PAN* image, $s_{XS_{ij}^{k}}^{2}$, is the variance of *XS* image in the *k*th band and $s_{PAN_{i,j}, XS_{i,j}^{k}}$, is the covariance of the *k*th band of *XS* image with *PAN* image. The above formulation applies for any pixel (*i,j*) within the $w \times w$ window defined around it. The larger the window, the more spatial contribution will be gained from the *PAN* image. This means that larger window size will produce spatially sharper fused images. However, larger window size will also result in degradation in the color. Therefore, there is a trade-off between spatial resolution gain and spectral content loss resulting from the window size. Hence, an optimal window size should be selected during the fusion process [21]. In this article for the possibility in comparison the results with the results that *Gungor* and *Shan* [21] have presented on their research, the window size was selected as 31×31.

Fig.s 10, 11, and 12 show the fused images with the *ST* fusion method with the 31×31 window size around of each pixel.

4. Combining IHS Fusion Method with ST Statistical Method

To improve the spectral quality of IHS fusion, we combined the IHS method with the ST method. In order to combine IHS method with ST method, XS image bands in Equation (3) are substituted with Intensity element, 'I', which is obtained from transforming RGB color space into IHS color space as in Equation (6). Accordingly, PAN image is fused just with Intensity element of XS image and produced the fused Intensity element of 'I*'. By substituting this fused Intensity element 'I*' in the reverse IHS transform and creating a new I*HS group and then doing the reverse IHS transform and transferring it into the RGB color space, the fused image through this combined method is obtained. This method is shown by IHS-ST symbol as follows.

$$I_{ij}^{*} = a_{ij} \times P_{ij} + b_{ij} \times I_{ij} \tag{6}$$

Due to this combination, Equations (4) and (5) are rewritten in the form of Equations (7) and (8), respectively.

$$m_{I^*_{ij}} = a_{ij} \times m_{P_{ij}} + b_{ij} \times m_{I_{ij}} = m_{I_{ij}} \qquad (7)$$

Where $m_{I^*_{ij}}$ is the average of fused Intensity element 'I*', $m_{P_{ij}}$ is PAN image average, and $m_{I_{ij}}$ is the average of Intensity element of XS image.

$$s^2_{I^*_{ij}} = (a_{ij})^2 s^2_{P_{ij}} + 2\times a_{ij}\times b_{ij}\times s_{P_{ij},I_{ij}} + (b_{ij})^2 s^2_{I_{ij}} = s^2_{P_{ij}} \qquad (8)$$

Where $s^2_{I^*_{ij}}$ is the variance of fused Intensity 'I*', $s^2_{P_{ij}}$ is PAN image variance, $s^2_{I_{ij}}$ is the variance of Intensity of XS image and $s_{P_{ij},I_{ij}}$ is the covariance of Intensity element of XS and PAN images. To calculate a^k_{ij} and b^k_{ij} coefficients, Equations (7) and (8) are used to obtain a second degree equation in terms of coefficient b_{ij} by substituting Equation (9). According to Equation (7), it can be written as:

$$a_{ij} = \frac{m_{I_{ij}}}{m_{P_{ij}}}\times(1-b_{ij}) = M\times(1-b_{ij}) \quad \& \quad M = \frac{m_{I_{ij}}}{m_{P_{ij}}} \qquad (9)$$

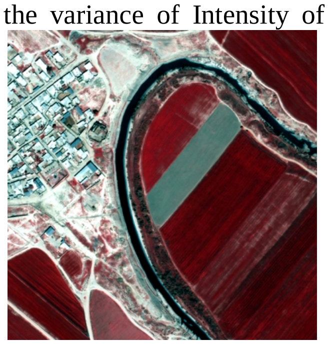

Fig 7: QuickBird Fused image using IHS method

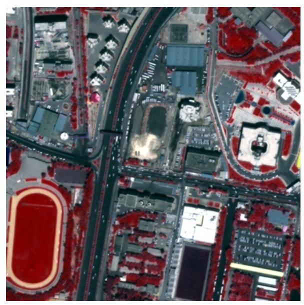

Fig 8: WorldView-02 Fused image using IHS method

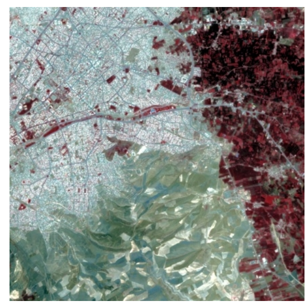

Fig 9: EO1-ALI-PAN and Landsat TM5 Fused image using IHS method

Fig. 10: QuickBird fused image using ST method

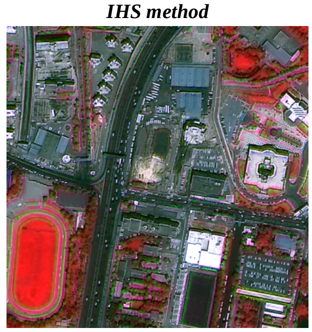

Fig. 11: WorldView-02 fused image using ST method

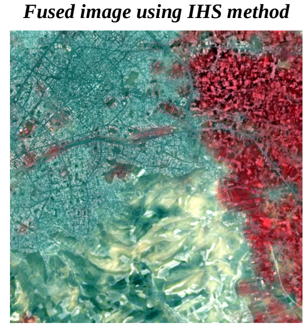

Fig. 12: EO1-ALI-PAN and Landsat TM5 fused image using ST method

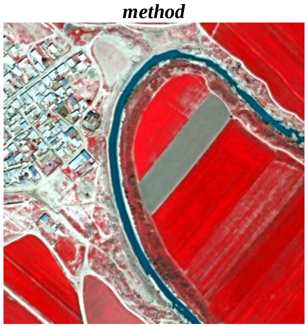

Fig. 13: QuickBird fused images using combined IHS-ST method

Fig. 14: WorldView-02 fused images using combined IHS-ST method

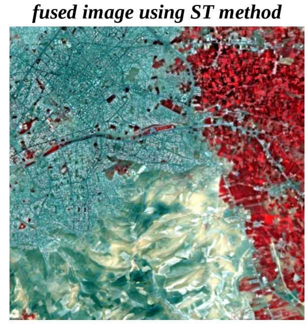

Fig. 15: EO1-ALI-PAN and Landsat TM5 fused images using combined IHS-ST method

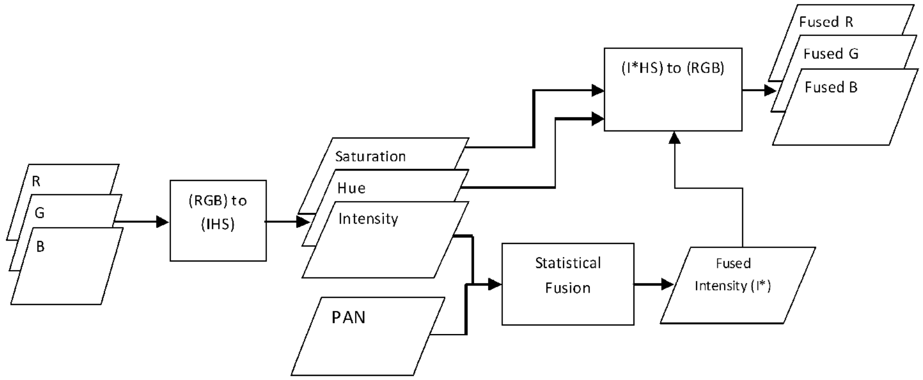

Fig. 16. The flowchart of IHS-ST combined image fusion method

By substituting a_{ij} coefficient from Equation (9) into Equation (8), a second degree equation in terms of coefficient b_{ij} is obtained.

$$\left(M^2 s_{P_{ij}}^2 + s_{I_{ij}}^2 - 2M\, s_{P_{ij}I_{ij}}\right)\left(b_{ij}\right)^2 + \left(2M\, s_{P_{ij}I_{ij}} - 2M^2 s_{P_{ij}}^2\right) b_{ij} + \left(M^2 - 1\right) s_{P_{ij}}^2 = 0 \quad (10)$$

By solving Equation (10), two answers are obtained for b_{ij} and as a consequence by substituting those into Equation (9), two answers are calculated for a_{ij} coefficient. Noticing that the aim of combining *PAN* image and Intensity element of *XS* image is to transfer the spatial information of *PAN* image into Intensity element of *XS* image, so from among two obtained answers for b_{ij} coefficient, the one which maximize the coefficient a_{ij} and as a result, increases the effect of *PAN* image in the fused image is chosen to be used in fusion process. In some cases, a_{ij} and b_{ij} coefficients are complex numbers. Under such circumstance, the real components of the complex roots are taken as a_{ij} and b_{ij} coefficients, since they can make Equation (10) closest to zero in the domain of real roots [21]. Fig.s 13, 14, and 15 show the fused images by the combined *IHS-ST* combined method. Fig. 16 shows the flowchart of this combined method.

5. Spectral Quality Assessment of the Fused Images

As the aim of this article is the spectral improvement of the conventional IHS methods by hybrid IHS-ST fusion method, so in this study some statistical indices were used for spectral quality assessment of the fused images. The aim of studying spectral quality is to measure the degree of spectral similarity between a fused image and main XS image. For spectral quality assessment of the fused image, apart from visual study as a necessary step, a series of numeral and statistical indexes such as Inter-Band Correlation Coefficient Bias (IBCCB), Cross-Band Correlation Coefficient (CBCC), Root Mean Square Error (RMSE), Signal to Noise Ratio (SNR), Normalized Mean Absolute Error (NMAE), and Spectral Angle Mapper (SAM) were used in this study. Besides the IHS, ST and IHS-ST methods, for comparison, we are provided the fused images with three other common fusion methods: Principle Component Analysis (PCA) [3,4,22], Brovey Transform [3,4,22] and Additive Shift Invariant Wavelet Transform (ASIWT) fusion methods [23-27]. The fused images using PCA, Brovey and ASIWT fusion methods have been shown in Fig.s 17-25 respectively.

5.1 Visual Study of Fused Images

As a necessary step in quality assessment of fused images we visually explored the fused images by the IHS, ST and IHS-ST methods [2,28]. Visual inspection of the fused images shows that the visual quality of fused images by IHS-ST method did not disturb in fusion process and fused images by this method have similarity to the original XS image. Also no color spreading exists in the fused images by this method such as the color spreading exists in the fused images by the ST method.

5.2 Inter-Band Correlation Coefficient Bias (*IBCCB*)

Correlation coefficient (CC) between two variables A and B (in this case two image bands having dimensions M×N) is defined as Equation (11) and reflects the correlation complete non-homogeneity for value (-1) and also complete similarity between two images for value (+1).

$$CC_{AB} = \frac{\sum_{i=1}^{M}\sum_{j=1}^{N}\left(A_{ij}-\bar{A}\right)\left(B_{ij}-\bar{B}\right)}{\sqrt{\sum_{i=1}^{M}\sum_{j=1}^{N}\left(A_{ij}-\bar{A}\right)^{2}\sum_{i=1}^{M}\sum_{j=1}^{N}\left(B_{ij}-\bar{B}\right)^{2}}} \qquad (11)$$

The IBCCB is calculated with Equation (12) as a spectral distortion index between the two bands of XS image (XS and XSj) and the corresponding

Fig. 17: QuickBird fused image using PCA method

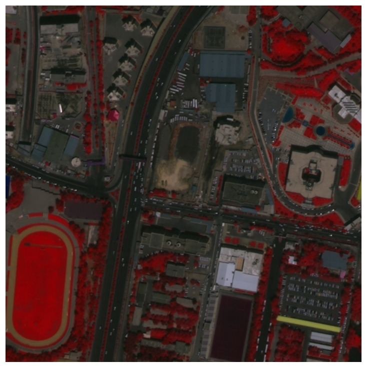

Fig. 18: WorldView-02 fused image using PCA method

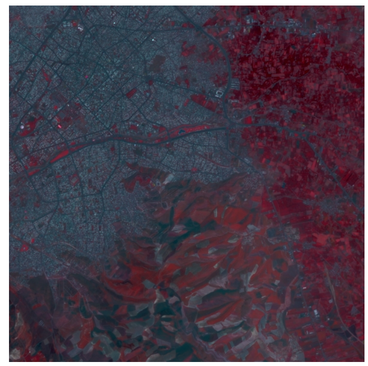

Fig. 19: EO1-ALI-PAN and Landsat TM5 fused image using PCA method

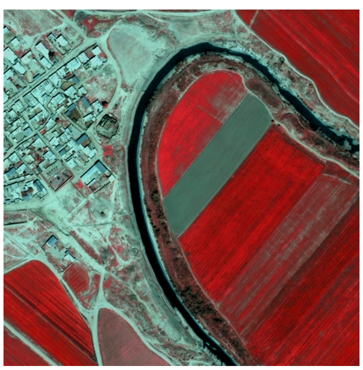

Fig. 20: QuickBird fused image using Brovey method

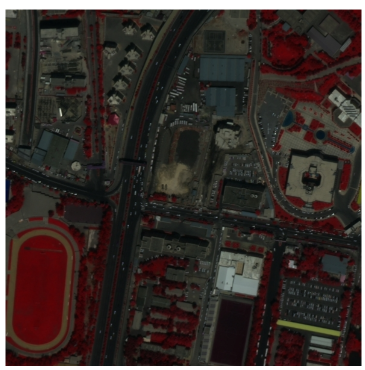

Fig. 21: WorldView-02 fused image using Brovey method

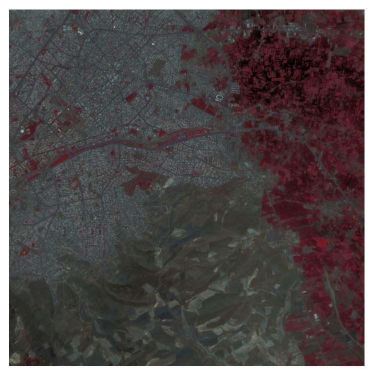

Fig. 22: EO1-ALI-PAN and Landsat TM5 fused image using Brovey method

Fig. 23: QuickBird fused image using ASIWT method

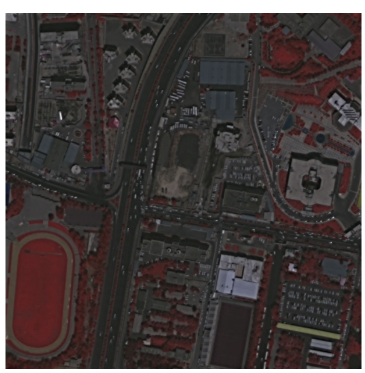

Fig. 24: WorldView-02 fused image using ASIWT method

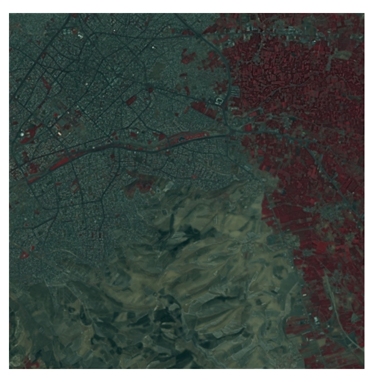

Fig. 25: EO1-ALI-PAN and Landsat TM5 fused image using ASIWT method

bands in the fused image (Fi and Fj) [30].

The ideal condition is when the IBCCB value is approaching to zero.

$$IBCCB_{ij} = CC_{XS_{ij}} - CC_{F_{ij}} \tag{12}$$

TABLE II shows the amount of IBCCB values between fused images' bands and XS images' bands. It is clear from TABLE II that combined IHS-ST method makes an improvement in the IBCCB index of the fused images in comparison with IHS and other methods especially between NIR Band and other two Red and Green bands.

5.3 Cross-Band Correlation Coefficient (*CBCC*)

Another index to measure the spectral quality of the fused image is the calculation of the correlation coefficient between fused image's bands and its corresponding bands in XS image i.e. CBCC [28,30,31]. Much closer this value to (+1), there will be a more similarity between bands of fused image and XS image. To calculate this index, Equation (12) is also used with variable A from XS image and variable B from fused image. According to Zhang [28] this is the most reliable quantitative criterion in comparing the quality of two images. In TABLE III, it can be seen that the CBCC values of combined IHS-ST method is closer than IHS and ST methods' values to (+1) especially in NIR band.

5.4 Root Mean Square Error (*RMSE*)

RMSE is a statistic of objective fidelity of fused image for assessing loss of the information in comparison with original XS image [32] and is calculated by Equation (13). This index measures the average amount of changes on any pixel caused by processing and are used to evaluate the similarity between the reference image XS and the fused image F [33]. The ideal value for this index is zero.

$$RMSE^{k} = \sqrt{\frac{\sum_{i=1}^{N}\sum_{j=1}^{M}\left(XS_{ij}^{k} - F_{ij}^{k}\right)^{2}}{N \times M}} \tag{13}$$

This index is a better criterion than CBCC and has more sensitivity [34]. Therefore if the quality of two different fusion methods regarding to Pearson's correlation coefficient is the same, then the RMSE index can be used to determine the better method. As it is seen in TABLE IV, the RMSE of IHS-ST method compared to IHS and ST methods especially in NIR band are much less.

Signal to Noise Ratio (SNR) If fused image F, is considered to be the sum of the original XS image and a noise signal e, then the root mean square of Signal to Noise Ratio for fused image F, is denoted as SNRrms and is calculated by Equation (14):

$$SNR_{rms}^{k} = \sqrt{\frac{\sum_{i=1}^{N}\sum_{j=1}^{M}\left(F_{ij}^{k}\right)^{2}}{\sum_{i=1}^{N}\sum_{j=1}^{M}\left(XS_{ij}^{k} - F_{ij}^{k}\right)^{2}}} \tag{14}$$

This is a subjective fidelity criteria measuring image quality by subjective evaluation of a human observer [32] and is commonly used in assessing image fusion techniques [35]. The bigger is the value of SNRrms the better is the quality of the fused image. TABLE V shows the value of this index for the fused images. As it can be seen the SNRrms values for IHS-ST methods is better than IHS method and has especial improvement in NIR band.

5.5 Normalized Mean Absolute Error (*NMAE)*

The index NMAE measures the relative deviation of the fused image from the XS image and is calculated by Equation (15). A smaller NMAE implies the better spectral quality of the fused image [36]. As it is shown in TABLE VI, the NMAE value for IHS-ST method is much smaller than IHS method.

$$NMAE = \frac{1}{M \times N}\sum_{i=1}^{M}\sum_{j=1}^{N}\frac{\left|F_{ij} - XS_{ij}\right|}{XS_{ij}} \tag{15}$$

Spectral Angle Mapper (SAM)

If each pixel values of XS image bands and its corresponding in the fused image are indicated with vectors V1(a,b,…,n) and V2(a',b',…,n') in which (a, b ,…,n) and (a', b', ..., n') are the gray values through band-1 to band-n, then the SAM denotes the value of the angle between these two vectors using Equation (16) [37].

$$SAM = arc\cos\left(\frac{\langle \vec{V}_1, \vec{V}_2 \rangle}{|\vec{V}_1||\vec{V}_2|}\right) \tag{16}$$

In Equation (16) $\langle \vec{V}_1, \vec{V}_2 \rangle$ is stands for the inner product of the vectors and symbol ($|\vec{V}|$) is stands for the vector length.

For two similar bands of XS and fused image F, the SAM(XS, F) index is defined according to Equation (16) as the E[SAM(a, b)], where E denotes Expectation and a and b denotes the generic pixel vector element of multispectral image XS and F, respectively [37]. SAM is a global spectral distortion index and measures the average spectral distortion. The closer to zero the SAM value the more similar are images XS and F [37].

TABLE VII shows the SAM index values for different fusion methods discussed in this article. The combined IHS-ST method has better values than the IHS and especially ST methods.

6. CONCLUSION

According to the results shown in TABLEs II up to VII, the spectral quality of the images fused through IHS-ST hybrid method presented in this article is much better than the spectral quality of the images fused through conventional IHS method and also other methods, especially in NIR band. On the other hand the spectral quality of the IHS-ST method is better than the quality of ST statistical method and also the amount of computation is near to one third of ST method. Also the results of TABLEs II up to VII for EO1-ALI-PAN and Landsat TM5 data set, show this method has not any problem in the fusion of images from different sensors.

table ii: Inter-Band Correlation Coefficient Bias Index (IBBCCB)

	QB			ALI-TM			WV-02		
	B4-B3	B4-B2	B3-B2	B4-B3	B4-B2	B3-B2	B7-B5	B7-B3	B5-B3
IHS	0.9754	1.0168	0.0054	0.6240	0.6800	0.0065	0.2993	0.2549	0.0069
ST	0.2675	0.2964	0.0022	0.2294	0.3462	-0.0254	0.1838	0.1727	-0.1327
IHS-ST	0.2364	0.2518	0.0022	0.1882	0.2466	-0.0046	0.1160	0.1086	0.0018
PCA	0.6783	0.6893	-0.0076	-0.4343	-0.3828	-0.0013	-0.1796	-0.1801	-0.0101
Brovey	0.2631	0.3139	0.0042	0.3143	0.4330	-0.0030	0.1400	0.1122	0.0027
ASIWT	0.3380	0.3584	0.0015	0.2080	0.2943	-0.0131	0.2548	0.2264	0.0095

table iii: Cross-Band Correlation Coefficient Index (CBCC)

	QB			ALI-TM			WV-02		
	B4	B3	B2	B4	B3	B2	B7	B5	B3
IHS	0.5479	0.9399	0.9225	-0.0569	0.7508	0.7370	0.8505	0.9649	0.9380
ST	0.8642	0.9376	0.9260	0.6334	0.8426	0.7271	0.7914	0.6539	0.9338
IHS-ST	0.9156	0.9608	0.9595	0.6747	0.8935	0.8373	0.9480	0.9638	0.9410
PCA	0.9938	0.7281	0.7212	0.9556	0.5883	0.6256	0.9726	0.9476	0.9474
Brovey	0.9094	0.9259	0.9079	0.1907	0.7334	0.6914	0.9421	0.9675	0.9451
ASIWT	0.8890	0.9439	0.9389	0.8440	0.9272	0.8496	0.9026	0.8935	0.9248

table iv: Root Mean Square Error Index (RMSE)

	QB			ALI-TM			WV-02		
	B4	B3	B2	B4	B3	B2	B7	B5	B3
IHS	67.5653	33.3071	34.4820	22.2501	16.5834	13.5060	9.1597	4.5541	8.0097
ST	24.0253	24.9779	26.0937	11.1674	10.7958	10.0267	11.3421	12.8021	6.8076
IHS-ST	19.2380	20.8176	20.0007	10.3613	9.2733	7.6321	5.4543	4.0017	6.6553

PCA	5.3579	50.7420	49.3020	9.7475	20.0243	20.4951	18.9136	15.2459	20.6637
Brovey	54.9597	32.5916	35.2758	17.2968	14.9035	15.9216	9.4657	12.4420	25.6895
ASIWT	23.0402	32.0536	32.3577	22.0082	7.1454	8.5121	12.5402	17.9883	11.7286

table v: Signal to Noise Ratio Index (snrrms)

	QB			**ALI-TM**			**WV-02**		
	B4	**B3**	**B2**	**B4**	**B3**	**B2**	**B7**	**B5**	**B3**
IHS	1.8759	3.4866	3.1842	2.9175	3.7767	3.7677	5.0789	7.7456	7.3725
ST	7.2415	5.1635	4.7214	6.5215	6.0155	5.2524	4.4087	2.8627	8.8443
IHS-ST	9.0348	6.2827	6.2073	7.0156	7.0741	6.9285	9.0426	8.9324	9.0868
PCA	31.8191	2.6823	2.6487	6.7216	2.7300	3.3100	3.5087	3.1708	2.1300
Brovey	2.2117	3.3292	2.8096	3.9091	4.1527	3.8528	5.4159	3.4995	1.4956
ASIWT	6.9873	3.7566	3.6764	2.3864	8.8176	6.6710	4.6969	2.8605	4.3376

table vi: Normalized Mean Absolute Error Index (nmae)

	QB			**ALI-TM**			**WV-02**		
	B4	**B3**	**B2**	**B4**	**B3**	**B2**	**B7**	**B5**	**B3**
IHS	0.3447	0.3430	0.3431	0.2342	0.2339	0.2338	0.1088	0.1090	0.1085
ST	0.5891	0.2326	0.2642	0.1190	0.1501	0.1547	0.1736	0.2752	0.0750
IHS-ST	0.0767	0.0811	0.0810	0.1098	0.1094	0.1094	0.0739	0.0733	0.0728
PCA	0.2429	1.0592	1.1241	0.1310	0.2329	0.3537	0.2740	0.3433	0.3820
Brovey	0.3451	0.1883	0.2110	0.1719	0.1719	0.2410	0.1662	0.2730	0.4789
ASIWT	1.5485	0.6400	0.7631	0.3024	0.0966	0.1289	0.2461	0.5558	0.1861

table vii: Spectral Angle Mapper Index (sam)

	QB	**ALI-TM**	**WV-02**
IHS	0.3108	0.2383	0.2655
ST	4.3057	3.0380	6.5371
IHS-ST	0.0796	0.1654	0.2401
PCA	13.0191	12.3263	18.9484
Brovey	5.1329	4.7451	17.8081
ASIWT	9.2344	10.6431	13.9820

7. REFERENCES

[1] T. Ranchin, B. Aiazzi, L. Alparone, S. Baronti, and L. Wald, "Image fusion – ARSIS concept and some successful implementation schemes," *ISPRS Journal of Photogrammetry and Remote Sensing*, vol. 58, no. 12, Jun. 2003, pp. 4–18.

[2] L. Wald, T. Ranchin, and M. Mangolini, "Fusion of satellite images of different spatial resolutions: Assessing the quality of resulting images," *Photogrammetric Engineering and Remote Sensing*, vol. 63, no. 6, Jun. 1997, pp. 691–699.

[3] C. Pohl, and J. L. Van Genderen, "Multisensor image fusion in remote sensing: Concepts, methods and applications," *International Journal of Remote Sensing*, vol. 19, no. 5, 1998, pp. 823–854.

[4] T. M. Tu, S. C. Su, H. C. Shyu, and P. S. Huang, "A new look at IHS-like image fusion methods," *Information Fusion*, vol. 2, no. 3, Sep. 2001, pp. 177-186.

[5] T. M. Tu, P. S. Huang, C. L. Hung, and C. P. Chang, "A fast Intensity-Hue-Saturation fusion technique with spectral adjustment for IKONOS imagery," *IEEE Geoscience and Remote Sensing Letters*, vol. 1, no. 4, Oct. 2004, pp. 309-312.

[6] F. A. Al-Wassai, N. V. Kalyankar, A. A. Al-Zuky, "The IHS transformations based image fusion," *Journal of Global Research in Computer Science*,vol. 2, no. 5, May 2011, pp. 70-77.

[7] E. M. Schetselaar, "Fusion by the IHS transform: Should we use cylindrical or spherical coordinates?," *International Journal of Remote Sensing*, vol. 19, no. 4, pp. 759–765, 1998.

[8] A. R. Smith, "Color gamut transform pairs," *Computer Graphics*, vol. 12, no. 3, Aug. 1978, pp. 12–19.

[9] W. K. Pratt, *Digital image processing: PIKS Scientific inside*, 4th ed. Hoboken: John Wiley & Sons, 2007, p. 84.

[10] J. Nunez, X. Otazu, O. Fors, A. Prades, V. Pala, and R. Arbiol, "Multiresolution-based image fusion with additive wavelet decomposition," *IEEE Transactions on Geoscience and Remote Sensing*, vol. 37, no. 3, May 1999, pp. 1204–1211.

[11] R. Haydn, G. W. Dalke, J. Henkel, and J. C. Bare, “Application of the IHS color transform to the processing of multisensor data and image enhancement,” in *Proc. Remote Sensing of Arid and Semi-Arid Lands*, Cairo: ISRS, 1982, pp. 599-616.

[12] D. A. Yocky, “Image merging and data fusion by means of the two-dimensional wavelet transform,” *Journal of the Optical Society of America*, vol. 12, no. 9, Sep. 1995, pp. 1834–1845.

[13] P. S. Chavez, S. C. Sides, and J. A. Anderson, “Comparison of three different methods to merge multiresolution and multispectral data: Landsat TM and SPOT panchromatic,” *Photogrammetric Engineering and Remote Sensing*, vol. 57, no. 3, Mar. 1991, pp. 295-303.

[14] Y. Zhang, “Problems in the fusion of commercial high-resolution satellite images as well as Landsat 7 images and initial solutions,” *International Archives of the Photogrammetry and Remote Sensing*, vol. 34, no. 4, Jul. 2002.

[15] X. Otazu, A. M. Gonzalez, O. Fors, and J. Nunez, “Introduction of sensor spectral response into image fusion methods. Application to wavelet-based methods,” *IEEE Transactions on Geoscience and Remote Sensing*, vol. 43, no. 10, Oct. 2005, pp. 2376–2385.

[16] Y. Zhang, “Understanding image fusion,” *Photogrammetric Engineering and Remote Sensing*, vol. 70, no. 6, Jun. 2004, pp. 657–661.

[17] M. González-Audícana, J. L. Saleta, O. G. Catalán, and R. García, "Fusion of multispectral and panchromatic images using improved IHS and PCA mergers based on wavelet decomposition," *IEEE Transactions on Geoscience and Remote Sensing*, vol. 42, no. 6, Jun. 2004, pp. 1291-1299.

[18] Y. Chibani and A. Houacine, "The joint use of IHS transform and redundant wavelet decomposition for fusing multispectral and panchromatic images," *International Journal of Remote Sensing.*, vol. 23, Sep. 2002, pp. 3821-3833.

[19] M. Choi, "A new Intensity-Hue-Saturation fusion approach to image fusion with a Tradeoff Parameter", *IEEE Transactions on Geoscience and Remote Sensing*, vol. 44, no. 6, Jun. 2006, pp. 1291-1299.

[20] G. P. Lemeshewsky, “Multispectral image sharpening using a shift-invariant wavelet transform and adaptive processing of multiresolution edges,” in *Proc. SPIE: Visual Information Processing 11th*, vol. 4736, Jul. 2002, pp. 189-200.

[21] O. Gungor, and J. Shan, “A statistical approach to multiresolution image fusion,” in *Proc. Pecora16, Global Priorities in Land Remote Sensing*, Sioux Falls, SD, Oct. 2005.

[22] A. Shamshad, W.M.A. Wan Hussin, and S.A., Mohd Sanusi, “Comparison of different data fusion approaches for surface features extraction using Quickbird images,” in *Proc. GISIDEAS*, Hanoi, Sep. 2004.

[23] A. R. Afary, M. J. Valadanzoj, M. Mohammad karim, “Satellite image fusion using wavelets transform,” in *Proc. 2nd International Conference of Machine Vision and Image Processing*, Tehran, Feb. 2003.

[24] D. E. Nirmala, B. S. Paul, V.Vaidehi, “A novel multimodal image fusion method using shift invariant discrete wavelet transform and support vector machines,” in *Proc. ICRTIT in Recent Trends in Information Technology*, Chennai, Jun. 2011, pp. 932 – 937.

[25] O. Rockinger, “Image sequence fusion using a shift invariant wavelet transform,” *in Proc. ICIP on Image Processing*, Santa Barbara, 1997, pp. 288 – 291.

[26] Y. Q. Li, L. L. Li, B. Li, “Objective evaluation of several shift invariant image fusion methods,” in *Proc. ICICSE in Science and Engineering*, Harbin , 2008., pp. 98 – 101.

[27] K. Amolins, , Y. Zhang , P. Dare, “Wavelet based image

[28] fusion techniques - An introduction, review and comparison,” *ISPRS Journal of Photogrammetry and Remote Sensing*, vol. 62, no. 4, Sep. 2007, pp. 249–263.

[29] Y. Zhang, “Methods for image fusion quality assessment - A review, comparison and analysis,” *International Archives of the Photogrammetry, Remote sensing and Spatial Information Sciences*, vol. 37, no. 7, Jul. 2008, pp. 1101-1109.

[30] W. Shi, C. Zhu, Y. Tian, and J. Nichol, “Fusing IKONOS images based on four-band wavelet transformation method,” *International Journal of Applied Earth Observation and Geoinformation*, vol. 6, no. 3-4, Mar. 2005, pp. 241-251.

[31] O. Gungor, and J. Shan, “Evaluation of satellite image fusion using wavelet transform,” in *Proc. 20th ISPRS Congress*, Istanbul, Jul. 2004.

[32] S. Klonus, and M. Ehlers, “Performance of evaluation methods in image fusion,” in *Proc. 12th IEEE Information Fusion*, Seattle, Jul. 2009, pp. 1409–1416.

[33] R. C. Gonzalez, and R. E. Woods, *Digital Image Processing*, 2nd ed. Upper Saddle River, Pearson Prentice Hall, 2002, pp. 419-420.

[34] L. Bao, D. Zhao, and D. Zhou, “Image fusion algorithm based on m-PCNN,” in *Proc. 2nd ETCS*, Wuhan, Mar. 2010, pp. 235–238.

[35] P. S. Pradhan, R. L. King, N. H. Younan, and D. W. Holcomb, “Estimation of the number of decomposition levels for a wavelet-based multiresolution multisensor image fusion,” *IEEE Transactions on Geoscience and Remote Sensing*, vol. 44, no. 12, Dec. 2006, pp. 3674–3686.

[36] T. Stathaki, *Image Fusion: Algorithms and Applications*, London, Academic Press, 2008, pp. 470-471.

[37] M. Costantini, A. Farina, and F. Zirilli, "The fusion of different resolution SAR images," in *Proc. IEEE*, vol. 85, no. 1, Jan. 1997, pp. 139-146.

[38] L. Alparone, L. Wald, J. Chanussot, C. Thomas, P. Gamba, and L. M. Bruce, "Comparison of pansharpening algorithms: Outcome of the 2006 GRS-S data-fusion contest," *IEEE Transactions on geoscience and remote sensing*, vol. 45, no. 10, Oct. 2007, pp. 3012–3021.